applied sciences

MDPI

Communication

The Saturation of the Response to an Electron Beam of Ce- and Tb-Doped GYAGG Phosphors for Indirect β-Voltaics

Petr Karpyuk [1], Mikhail Korzhik [1,2,*], Andei Fedorov [1,2], Irina Kamenskikh [3], Ilya Komendo [1], Daria Kuznetsova [1], Elena Leksina [3], Vialy Mechinsky [1,2], Vladimir Pustovarov [4], Valentina Smyslova [1], Vasilii M. Retivov [1], Yauheni Talochka [2], Dmitry Tavrunov [4] and Andrei Vasil'ev [5]

[1] National Research Center "Kurchatov Institute", 123098 Moscow, Russia
[2] Institute for Nuclear Problems, Belarus State University, 11 Bobruiskaya, 220030 Minsk, Belarus
[3] Faculty of Physics, Lomonosov Moscow State University, 119992 Moscow, Russia
[4] Experimental Physics Department, Ural Federal University, 620002 Yekaterinburg, Russia
[5] Skobeltsyn Institute for Nuclear Physics, Lomonosov Moscow State University, 119992 Moscow, Russia
* Correspondence: mikhail.korjik@cern.ch

Abstract: GYAGG:Tb (Ce) scintillators have been confirmed to be promising sources of light emission when excited by an intense 150 keV electron beam. The saturation of the scintillation yield under such excitation conditions has been studied. To explain the results obtained, a model that considers the Auger quenching mechanism was used. The Ce-doped material did not show saturation, whereas a moderate 30% drop of the yield was measured in the Tb-doped sample at the highest excitation beam intensity ~1 A/cm^2. This put forward a way to exploit the Tb-doped scintillator for indirect β-voltaic batteries.

Keywords: scintillation; quaternary garnet; terbium; light yield; decay time; saturation

check for updates

Citation: Karpyuk, P.; Korzhik, M.; Fedorov, A.; Kamenskikh, I.; Komendo, I.; Kuznetsova, D.; Leksina, E.; Mechinsky, V.; Pustovarov, V.; Smyslova, V.; et al. The Saturation of the Response to an Electron Beam of Ce- and Tb-Doped GYAGG Phosphors for Indirect β-Voltaics. *Appl. Sci.* **2023**, *13*, 3323. https://doi.org/10.3390/app13053323

Academic Editors: Shengchun Yang, Bin Wang and Hairui Cai

Received: 1 February 2023
Revised: 25 February 2023
Accepted: 26 February 2023
Published: 6 March 2023

1. Introduction

Radioisotope sources of electricity form a very useful class of micro power sources of energy, while many of them are devices that use the intermediate conversion of ionizing radiation energy into heat [1,2]. Alternative structures include isotope sources, which use the effect of ionization by corpuscular radiation of semiconductor converters to generate electricity [3–10]. Such an approach promises high efficiency; however, radiation damage to the semiconductor material becomes an almost insurmountable obstacle, negating the potential advantage of such a source—long service life. The problem can be solved by utilizing indirect converters, in which the photovoltaic semiconductor element and the isotope source are separated by a layer of high light yield and radiation-hard scintillation material [11–13]. Such requirements are met by crystalline compounds of the garnet structural type, activated by rare-earth elements [14]. Their radiation resistance under a different kind of ionizing radiation was confirmed in [15–18]. Tolerance to ionizing radiation occurs in garnets because the formed color centers have absorption bands primarily in the ultraviolet region and do not overlap the Ce3+ scintillation band of such materials, which is typically localized in the yellow-green region of the spectrum [19–21].

Among the currently developed crystalline scintillators with a garnet structure [22], the (Gd,Y)$_3$Al$_2$Ga$_3$O$_{12}$ materials activated by Ce and Tb ions have the highest scintillation yield. Activation with Ce ions leads to fast scintillation, which, however, is not a critical parameter for the considered application. Moreover, the scintillation of Ce ions experiences strong temperature quenching, which is not typical for scintillations of Tb ions in crystals of the same composition [23]. Luminescence bands of Tb ions located in the visible range originating from f-f transitions are parity and multiplicity forbidden. Their characteristic decay time is in the millisecond range. For such scintillators, upon intense excitation by ionizing radiation, an additional channel of luminescence quenching occurs by the Auger mechanism [24]. Such a mechanism may lead to a significant decrease in the luminescence yield and, consequently, to a decrease in the efficiency of the converter immediately after the start of its operation.

To elucidate the effects of saturation, we performed a direct measurement of the saturation of the scintillation yield in $(Gd,Y)_3Al_2Ga_3O_{12}$ ceramic samples activated with Ce and Tb ions using a 150 keV electron accelerator with intensity varied over a wide range. We focused on the samples activated with Tb ions, which were optimized to achieve the optimal concentration of the activator and the composition of the matrix of the quaternary garnet. A model of luminescence saturation in the considered compounds as a function of ionization density was developed. It satisfactorily describes the experimental data. The data obtained led us to the conclusion that the saturation effect will not lead to a significant change in the efficiency of the converter when widely used isotope sources for betavoltaic are used.

2. Sample Preparation and Measurements

Powder precursors of ternary garnets with variations in terbium concentration were produced by the reverse coprecipitation method. The precursors were calcined in corundum crucibles at the temperature of 850 °C for 2 h for garnet phase formation. After calcination, the powders were milled in a laboratory planetary mill (Retsch PM-100) in isopropanol media (median particle size, ~1.5 µm). Then, the powders were compacted in the shape of tablets with a diameter of 20 mm by uniaxial pressing at a pressure of 64 MPa (PLG-20 Laboratory Press by LabTools). The compacts were sintered in an air atmosphere at 1600 °C for 2 h using the Nabertherm LHT 02/17 LB high-temperature furnace. Ceramic samples were translucent; had >99.6% of theoretical density, which corresponds to the range of 5.84–5.89 g/cm^3 depending on composition; and had an optical transmission of 35–40% at 550 nm. The compositions of the samples and corresponding abbreviations are given in Table 1. Depending on terbium concentration, the elemental composition of the matrix slightly shifted. For Samples 1–4, the Gd/Y ratio in composition was chosen following the results described in [25]. Samples 5 and 6 were made to examine the possible influence of Gd/Y ratio deviation on the luminescence properties, whereas Sample 7 was solely doped with Ce. The Ce-doped sample was not codoped with Mg. Therefore, similarly to $Gd_3Al_2Ga_3O_{12}$:Ce and the other quaternary garnets, it demonstrated phosphorescence [14,26].

Table 1. Tb- and Ce-doped samples compositions.

#	Sample Composition	Abbreviation
1	$Gd_{1.175}Y_{1.775}Tb_{0.05}Al_2Ga_3O_{12}$	GYAGG:Tb, Tb = 0.05
2	$Gd_{1.160}Y_{1.740}Tb_{0.1}Al_2Ga_3O_{12}$	GYAGG:Tb, Tb = 0.1
3	$Gd_{1.120}Y_{1.730}Tb_{0.15}Al_2Ga_3O_{12}$	GYAGG:Tb, Tb = 0.15
4	$Gd_{1.100}Y_{1.700}Tb_{0.2}Al_2Ga_3O_{12}$	GYAGG:Tb, Tb = 0.2
5	$Gd_{1.4}Y_{1.4}Tb_{0.2}Al_2Ga_3O_{12}$	GYAGG:Tb-2, Tb = 0.2
6	$Gd_{1.1}Y_{1.7}Tb_{0.2}Al_2Ga_3O_{12}$	GYAGG:Tb-3, Tb = 0.2
7	$Gd_{1.175}Y_{1.777}Ce_{0.03}Al_2Ga_3O_{12}$	GYAGG:Ce, Ce = 0.03

The pure garnet phase of the samples was confirmed by the X-ray diffraction method (2D Phaser by Bruker with linearly polarized Cu radiation kα doublet 1.5406 and 1.5444 Å), as expected. The resulting ceramic samples were single phase with a garnet structure (Figure 1). The inset shows the evolution of the main peak of the XDR spectrum, indicating a slight variation connected with the terbium content in the ceramic.

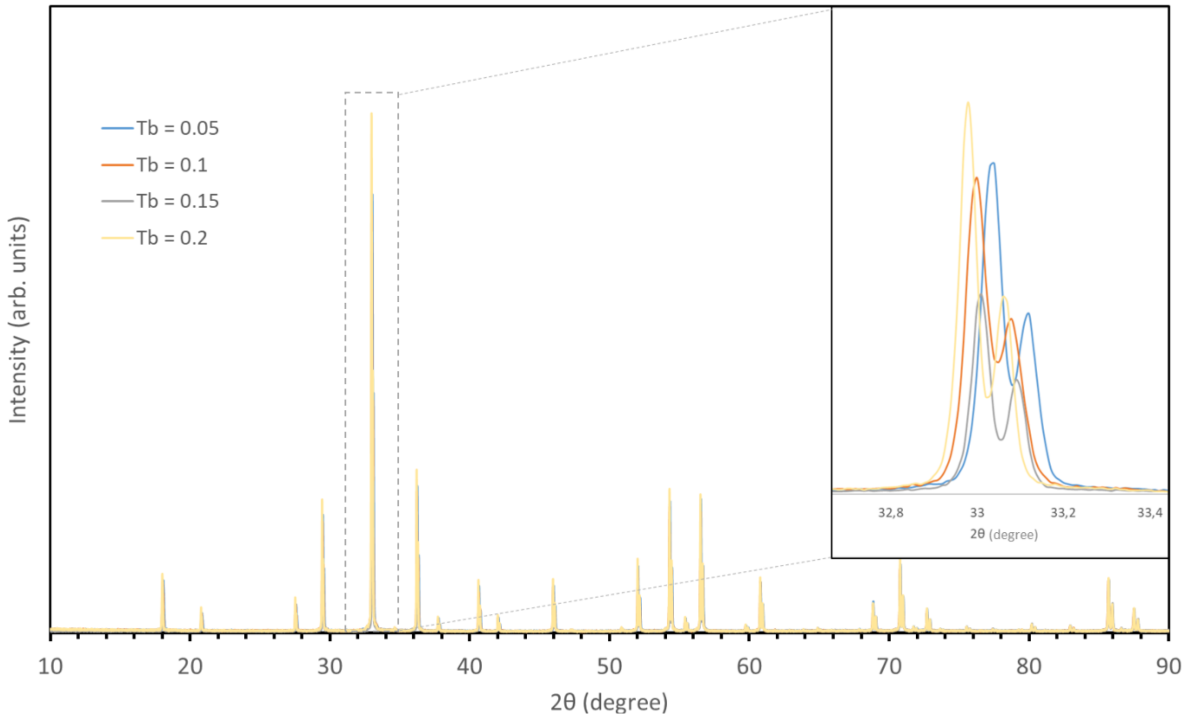

Figure 1. X-ray diffraction pattern of GYAGG:Tb ceramics samples with different terbium concentration.

The luminescence spectra during photoexcitation (PL) of the samples were measured with the Lumex FLUORAT-02-PANORAMA spectrofluorimeter at room temperature in the wavelength range of 360–700 nm with an excitation wavelength (λex) of 273 nm, which corresponds to the excitation in the $4f^7$-$5d^1f^6$- interconfiguration transition of Tb^{3+}-ions. The photoluminescence kinetics of the samples were measured with the PicoQuant Fluotime 200 fluorometer. The excitation of photoluminescence during the kinetics measurement was carried out using an LED with a wavelength of 270 nm and a pulse width (FWHM) shorter than 1 ns.

The scintillation intensity was evaluated at irradiation with the MIRA-2D small-size pulsed accelerator with the IMA-2-150E electron tube (150 keV; highest current density, 1 A/cm^2; pulse duration, ~20 ns). The beam repetition frequency was set as 10 Hz. It corresponds to the 1 cm^2 surface activity provided by a certain amount of the 100% enriched β-isotope as follows: ^{63}Ni-0.12g;^{147}Pm-0.0073g; ^{14}C-1.51g. Therefore, the measurements at the maximal current were performed in the irradiation conditions close to the conditions of further exploitation in the β-voltaic cells. To measure the scintillation yield at different intensities of the excitation, the current of the beam was attenuated with a set of foil absorbers. The scintillation spectra were recorded using the Oriel Instruments FICS 77443 spectrograph (uncooled CCD detector; spectral resolution, 2.4 nm; ~0.34 nm/pixel) by collecting the luminescence at ~45 degrees to the direction of the electron beam. The yield of the scintillation was defined as an integral under the radioluminescence curve. The absorbed dose during the exposure was measured by a SO PD (E) -1/10 "VNIIFTRI" certified film dosimeter, measuring the induced optical density at a wavelength of 550 nm. At an absorbed dose rate of 0.5 kGy/s, the absorbed dose was 2.0 kGy. The accelerator was used to measure the scintillation kinetics in different spectral ranges of the Tb-doped sample. The required wavelength was selected with a DMR-4 prismatic double monochromator. The Hamamatsu R6358-10 photomultiplier tube and TDS-2002 digital oscilloscope connected to a PC were used to record the scintillation pulse after a single accelerator pulse. Due to an identity of the luminescence properties of the samples the representative sample from the set, namely GYAGG:Tb, Tb = 0,15 was used for the measurements with excitation by the accelerator.

3. Results

The comparison of the PL spectrum measured at room temperature λex =273 nm, corresponding to the excitation in the 4f^7-5d^{1}f^6 interconfigurational transition of Tb^{3+} ions and the scintillation spectrum, is shown in Figure 2. For both types of excitations, the spectrum is typical for the luminescence of Tb^{3+} ions from two radiative states: $^5D_3 \rightarrow {}^7F_J$, and $^5D_4 \rightarrow {}^7F_J$. The luminescence spectra of GYAGG:Ce completely coincide with data published elsewhere [27,28]. The PL intensity increases in proportion to the concentration of the activator for transitions from the $^5D_4$ state but has the opposite trend for transitions from the $^5D_3$ state. The cross-relaxation process between neighboring Tb^{3+} ions depends on the concentration of the activator as shown in [29,30] and causes observed trends.

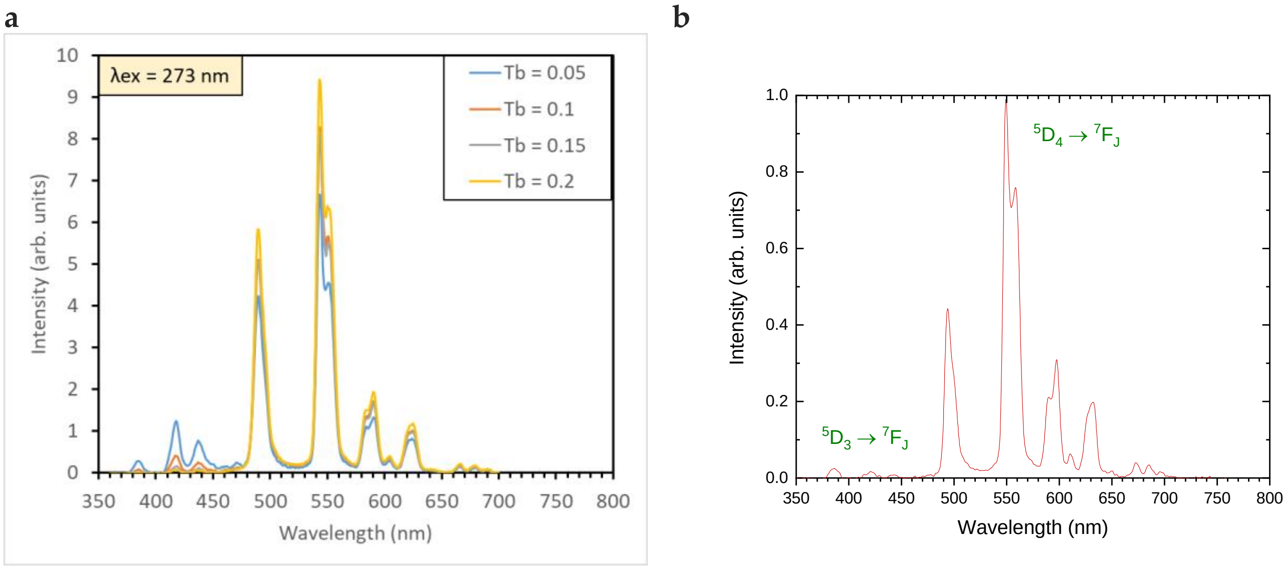

Figure 2. Room temperature PL spectra at excitation in Tb^{3+} interconfiguration transition (λex = 273 nm) of GYAGG:Tb samples versus the activator concentration (**a**); scintillation spectrum of the GYAGG:Tb, Tb = 0.15 at excitation by the electron beam at the maximum intensity (**b**).

The decay kinetics of PL in the region of the $^5D_4 \rightarrow {}^7F_J$ transition are shown in Figure 3. The kinetics of luminescence from the lower radiative state $^5D_4$ practically do not change, remaining close to the single exponential with a decay time of 3 ms. This indicates that no concentration quenching of $^5D_4 \rightarrow {}^7F_J$ luminescence is observed in the concentration range studied.

Similar results have been observed for the samples with a different ratio Gd/Y (samples GYAGG:Tb-2, Tb = 0.2 and GYAGG:Tb-3, Tb = 0.2). Figures 4 and 5 show the luminescence spectra and luminescence kinetics of the corresponding samples.

The PL intensity for sample GYAGG:Tb-2, Tb = 0.2 is approximately 20% lower than for sample GYAGG:Tb-3. Therefore, the ratio of components close to the latter composition was used in the concentration series.

The kinetics of scintillation at excitation by an electron-beam pulse were measured in the region of two radiative transitions $^5D_3 \rightarrow {}^7F_J$ (380 nm) and $^5D_4 \rightarrow {}^7F_J$, (546 nm). Figure 6 shows scintillation kinetics measured with GAYGG:Tb, Tb = 0.15.

The scintillation, which is caused by the $^5D_3 \rightarrow {}^7F_J$ transition, is strongly quenched by the nonradiative transfer from the $^5D_3$ to the $^5D_4$ state. As a result, there is a rising part in the kinetics of the scintillation in the spectral range of the $^5D_4 \rightarrow {}^7F_J$ transition with a constant of 150 μ. At a low excitation intensity, ~0.1 A/cm^2, the scintillation kinetics is close to that of photoluminescence; however, upon highest excitation, the decay constant decreases by ~20%, which is due to additional quenching. Figure 7 shows the dependences of the scintillation yield on the excitation intensity of GYAGG:Tb Tb = 0.15 and GYAGG:Ce measured at room temperature.

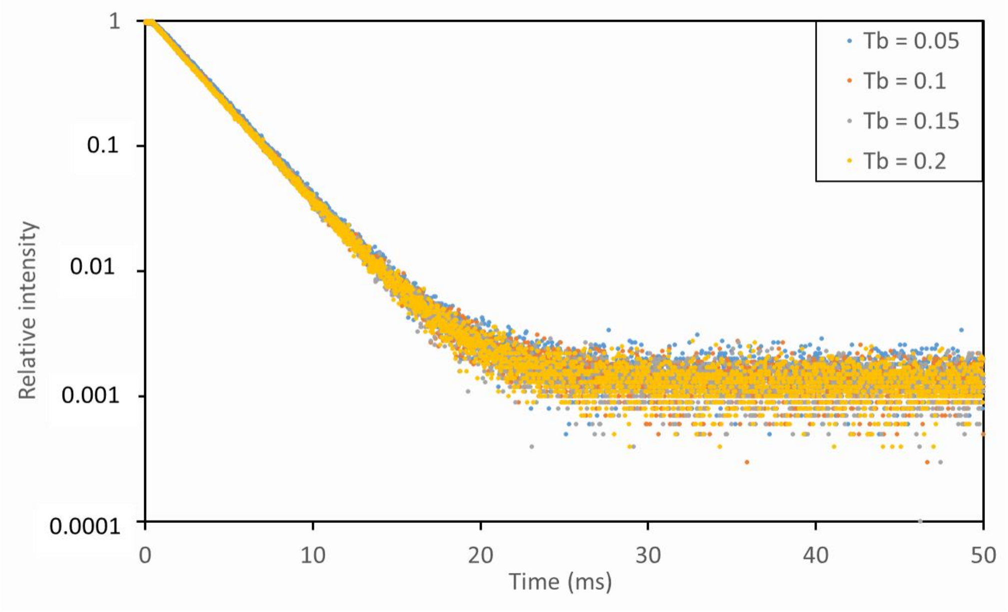

Figure 3. Room temperature PL kinetics $^5D_4 \rightarrow {}^7F_J$ (λreg = 546 nm) in GYAGG:Tb ceramic samples versus Tb content.

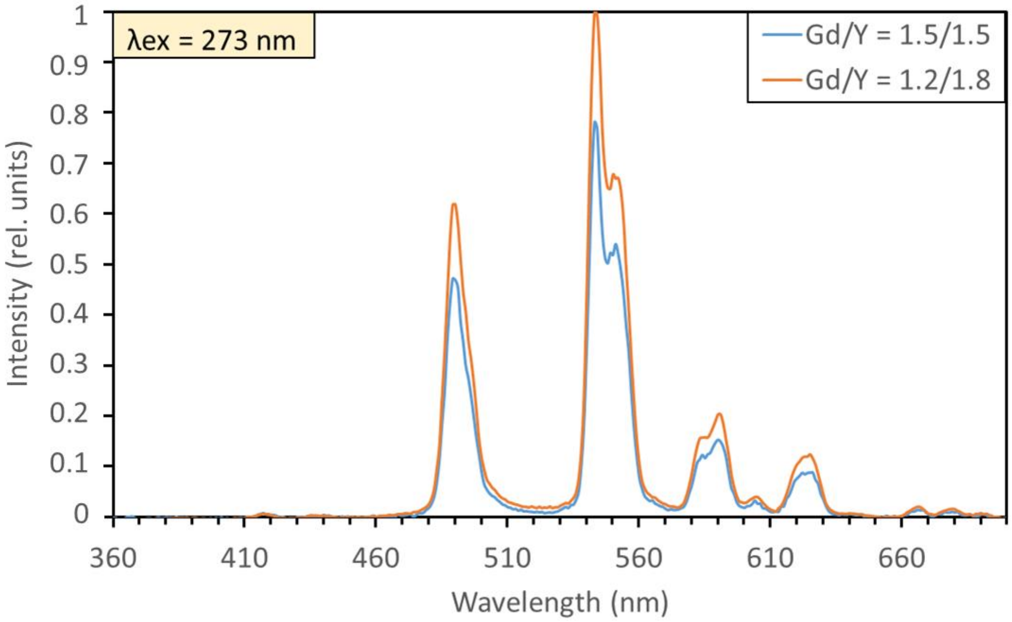

Figure 4. Room temperature PL spectra at excitation in Tb^{3+} interconfiguration transition (λex = 273 nm) of GYAGG:Tb-2 and GYAGG:Tb-3 samples. Inset includes the Gd/Y ratio, assuming a homogeneous distribution of the Tb ions between positions occupied by Gd and Y ions. Therefore, the Gd and Y indexes are each increased by 0.1.

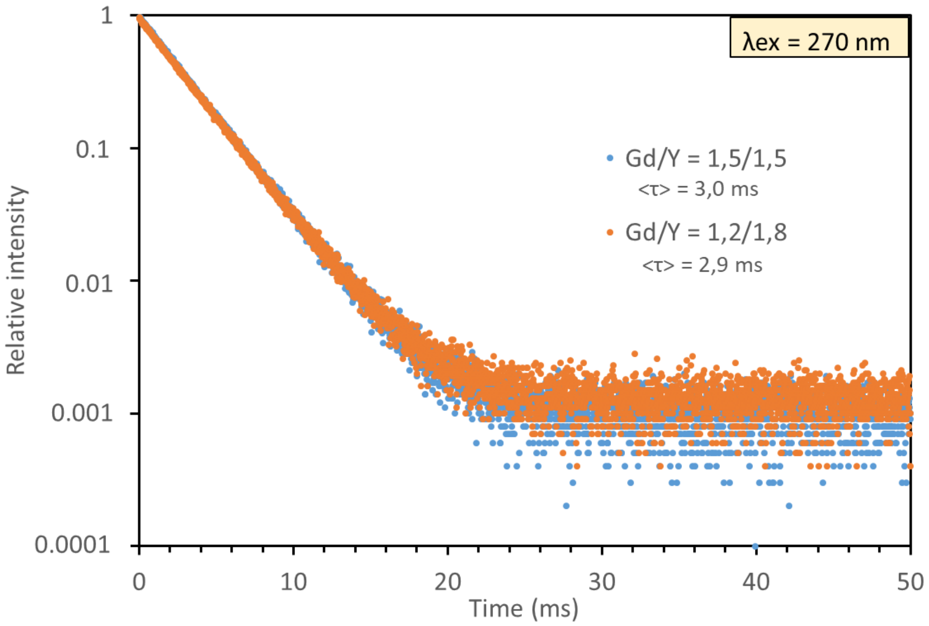

Figure 5. Room temperature PL kinetics $^5D_4 \rightarrow {}^7F_J$ (λreg = 546 nm) in GYAGG:Tb-2 и GYAGG:Tb-3, samples.

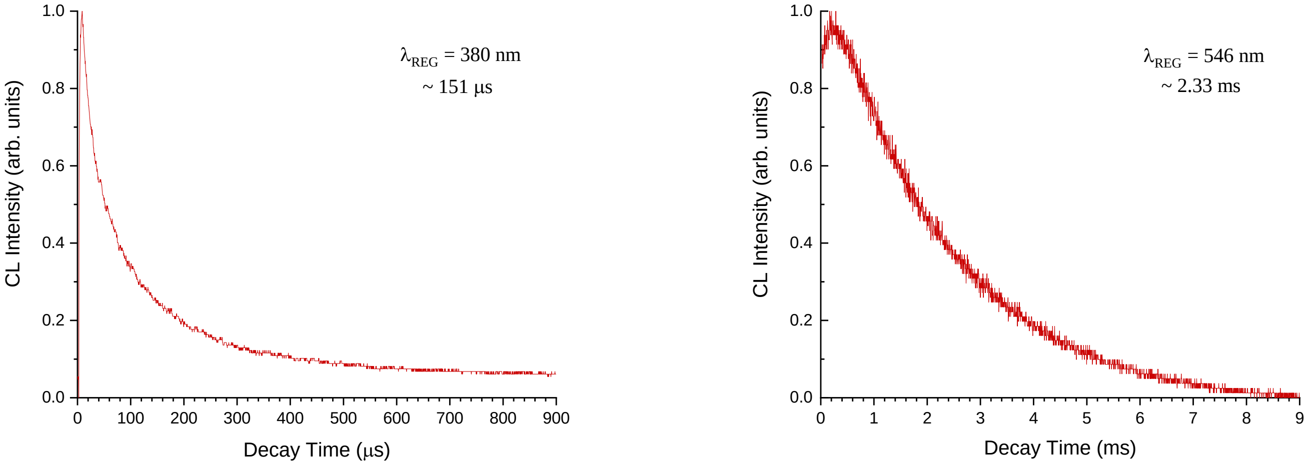

(**a**) (**b**)

Figure 6. Room temperature scintillation kinetics of GYAGG:Tb, Tb = 0.15, in the spectral range of the transitions: (**a**) $^5D_3 \rightarrow {}^7F_J$ (380 nm); (**b**) $^5D_4 \rightarrow {}^7F_J$; (546 nm).

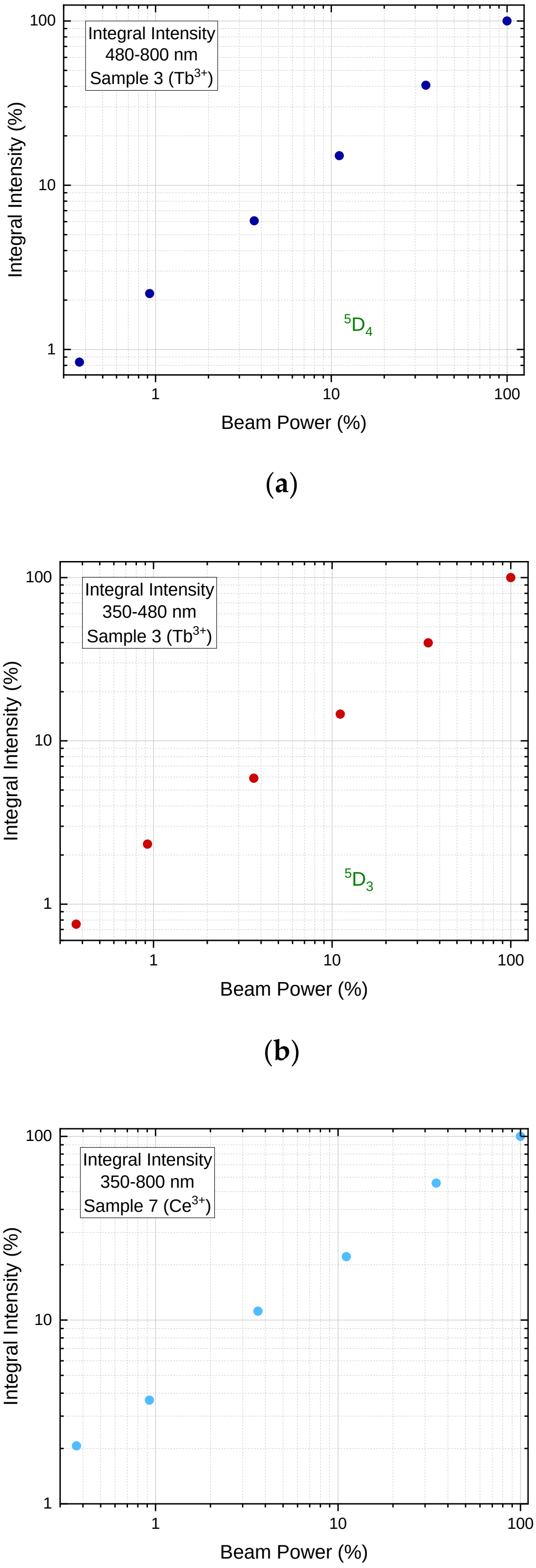

(**a**)

(**b**)

(**c**)

Figure 7. Normalized integrated intensity of the scintillation in the spectral range of the transitions: (**a**) $^5D_4 \rightarrow {}^7F_J$; (**b**) $^5D_3 \rightarrow {}^7F_J$ of GYAGG:Tb, Tb = 0.15; (**c**) GYAGG:Ce.

4. Discussion

Figure 7 demonstrates that there is a sublinear dependence of the scintillation yield on the accelerator current. To account for this effect, a model of saturation of the yield of scintillation in the GYAGG:Tb (Ce) crystal was developed. The saturation of the yield can have different origins: it can be due to the depletion of available radiative centers in the ground state or to the onset of the interaction of excited centers effectively limiting their output. Further, it will be shown that the former effect is not applicable to our results, but the latter one provides a reasonable agreement with experimental data. The model is applied to the results obtained with the $Gd_{1.120}Y_{1.730}Tb_{0.15}Al_2Ga_3O_{12}$ and $Gd_{1.175}Y_{1.777}Ce_{0.03}Al_2Ga_3O_{12}$ samples.

The saturation of the scintillation light yield in the crystal might be described in terms of kinetic equations. As a first step, the average concentration of electronic excitations in the region excited in the sample by the electron beam is to be estimated. The average length of the track created by the incident 150 keV electron in the GYAGG crystal was estimated using the GEANT4 package [31] to be 98 µm. The energy of about two values of the energy gap (i.e., ~12 eV) is required to create one electron–hole pair. Thus, the incident 150 keV electron can create up to 12,500 electronic excitations. The mean-free path of the secondary electrons can vary from 10 to 100 nm, thus the volume of one track can be about 3×10^{-7} to 3×10^{-5} cm^3. The number of the 150 keV electrons for the maximal electron-beam current is equal to $N_e^i = \frac{1\ A \cdot 20\ ns}{1.602 \cdot 10^{-19}\ C} = 1.24 \times 10^{11}$. For the electron-beam spot size on the sample of 1 cm^2 and penetration depth of about 70 µm (less than the track length since the track is not straight), the volume of the excited region of the sample is 0.007 cm^3. According to this estimate, the tracks are overlapping for the whole range of the available electron-beam current. For the current of 1 A, the number of electron–hole pairs created by the accelerator pulse is equal to 1.55×10^{15}, and their initial concentration for overlapping tracks is $n_{ex} = 2 \times 10^{17}$ cm^{-3}. The concentration of activator centers (Tb or Ce) in the GYAGG crystals is estimated to be $n_{Tb} = 6.7 \cdot 10^{20}$ CM^{-3} (for concentration equal to 0.15 Tb ions per formula unit, 5% sites are substituted by Tb) and $n_{Ce} = 1.34 \times 10^{20}$ CM^{-3} (for concentration equal to 0.03 Ce ions per formula unit, 1% sites are substituted by Ce). Thus, the concentration of activators (n_{Tb} or n_{Ce}) is substantially larger than the concentration of excitations n_{ex} produced by one electron-beam pulse. Therefore, we can neglect the saturation effects due to the exhausting of nonexcited activators. The decay time of the lowest radiative state of Tb ion in GYAGG crystal is known from the experimental results above. In addition, Tb can nonradiatively relax from the upper $^5D_3$ to the lower $^5D_4$ state with a decay time of 150 µs. The decay time of an excited Ce ion in GYAGG crystal was set to be 50 ns [32]. The separation between the pulses of the beam of 0.1 s is substantially larger than the decay time of the Tb (Ce) activator, thus all excited activator ions relax between two pulses.

The kinetic equations for Tb-doped GYAGG crystal can be written as follows:

$$\frac{dn_{Tb^5D_4}}{dt} = -\frac{1}{\tau_{Tb^5D_4}} n_{Tb^5D_4} + \frac{1}{\tau_{Tb^5D_3 \to Tb^5D_4}} n_{Tb^5D_3} - \beta_{Tb^* + Tb^*} n_{Tb^5D_4} n_{Tb^*}, \tag{1}$$

$$\frac{dn_{Tb^5D_3}}{dt} = -\frac{1}{\tau_{Tb^5D_3}} n_{Tb^5D_3} - \frac{1}{\tau_{Tb^5D_3 \to Tb^5D_4}} n_{Tb^5D_3} - \beta_{Tb^* + Tb^*} n_{Tb^5D_3} n_{Tb^*}, \tag{2}$$

$$n_{Tb^*} = n_{Tb^5D_4} + n_{Tb^5D_3} \tag{3}$$

Here, the radiative constants $\tau_{Tb^5D_4} = 3.0\ ms$. The radiative constant of $^5D_3$ is not known, so we chose for it to be equal to that of $^5D_4$: $\tau_{Tb^5D_3} = 3.0\ ms$. The effect of the exact value of this radiative constant is not critical for the solution of this set of equations since the characteristic time of nonradiative transfer from one state to the other is much smaller: $\tau_{Tb^5D_3 \to Tb^5D_4} = 150\ \mu s$. For the actual Tb concentration, the rate of Auger quenching for the pair of excited Tb ions $\beta_{Tb^* + Tb^*}$ was set as $0.1 \cdot 10^{-13} \frac{cm^3}{s}$, which corresponds to the best fit of the experimental result presented in Figure 8a. This value is noticeably smaller than the value $1.8 \cdot 10^{-13} \frac{cm^3}{s}$ for YAG:Tb (10%) reported in [24]. The initial conditions for the system (1–3) can be written as $n_{Tb^{5}D_3}(t=0) = n_{ex}(I) = I(A) \cdot 4.055 \cdot 10^{16}\ cm^{-3}$ and $n_{Tb^{5}D_4}(t=0) = 0$. The substantial difference between the Auger rate obtained here and in [24] is well explained by the different Tb concentration in these two cases (5% in the present work and 10% in [24]). The interaction between the two excited terbium ions is efficient only if the distance between them is about one nanometer, which is a characteristic value for dipole–dipole and exchange interaction. Such a small distance can be achieved either by a high density of excitation (which is not the case here) or after the diffusion of excitations towards each other. A smaller terbium concentration corresponds to a larger mean distance between two terbium ions. The diffusion coefficient of the excitations over the terbium subsystem or the probability of excitation hopping between terbium ions is also concentration dependent. A smaller terbium concentration is characterized by a larger distance between terbium ions and has two consequences: a smaller diffusion coefficient of excitations over the terbium subsystem and a smaller portion of closely spaced Tb pairs.

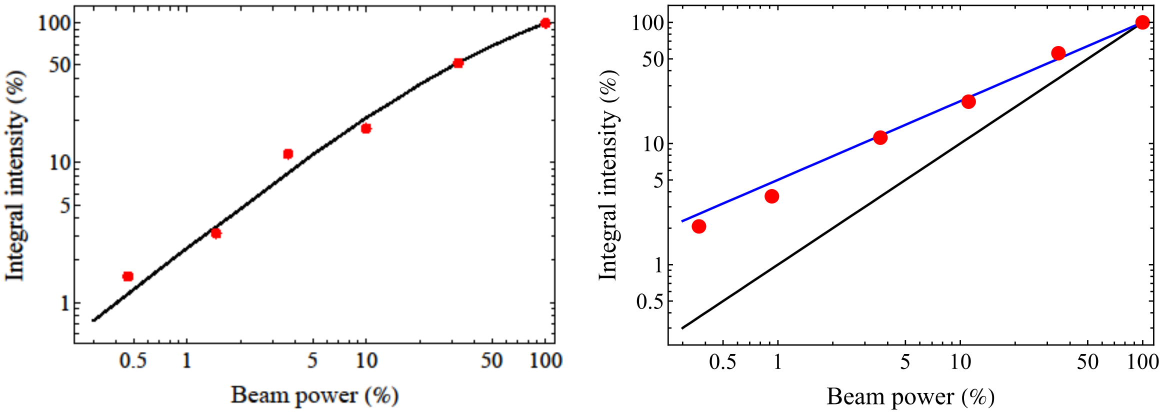

(**a**) (**b**)

Figure 8. Scintillation yield versus beam power: (**a**) GYAGG:Tb; (**b**) GYAGG:Ce.

The kinetic equation for Ce-doped GYAGG crystal can be written as follows:

$$\frac{dn_{Ce*}}{dt} = -\frac{1}{\tau_{Ce*}} n_{Ce*} - \beta_{Ce^*+Ce^*} n_{Ce*}^2 + i(t) \tag{4}$$

where $\tau_{Ce*} = 50\ ns$, $i(t) = \frac{n_{ex}(I)}{\sqrt{2\pi}\sigma} e^{-\frac{(t-\mu)^2}{2\sigma^2}}$ is the Gaussian source with $\sigma = \frac{20\ ns}{2.355} = 8.49\ ns$, and the rate of Auger quenching for pair of excited Ce ions $\beta_{Ce^*+Ce^*}$ was set as $0.7 \cdot 10^{-13} \frac{cm^3}{s}$. Meanwhile, the μ parameter of the Gaussian source $i(t)$ should be set quite large to consider $i(t=0) \approx 0$. In the current work, $\mu = 3\sigma$ was used. The initial condition can be set as $n_{Ce*}(t=0) = 0$. The solution to Equation (4) suggests a linear dependence of cerium luminescence yield on the beam current even for much higher values of the parameter $\beta_{Ce^*+Ce^*}$ up to $10^{-10} \frac{cm^3}{s}$, corresponding to nonrealistic values of the diffusion coefficient. We suppose that the Auger effect in the interaction of two excited cerium ions for 1% Ce concentration should be negligible.

Figure 8 presents the comparison of the experimentally measured and simulated normalized yield of scintillation in GYAGG:Tb, which includes transitions both from $^5D_3$ and $^5D_4$ excited states and GYAGG:Ce (b) as a function of the beam power. The scintillation yield of terbium-doped GYAGG ceramics is rather well described by the model (black line in Figure 8a). It indicates that the Auger mechanism of quenching dominates in the range of studied excitation power. The drop in the yield is defined at the level of 30%, which also correlates with the change in scintillation kinetics at maximum excitation intensity and is quite moderate.

For the Ce-activated sample, a deviation of the simulated dependence (black line in Figure 8b) and the line fitting the experimental data (blue line) is obvious, especially in the range of the low excitation power. Within the model, due to the short lifetime of the excited state of the Ce^{3+} ions, the scintillation yield should weakly depend on the excitation power, and the yield versus power curve should be close to a straight line. A straight line also satisfactorily approximates the experimental data, and the difference in the range of low excitation intensities is due to the phosphorescence, as mentioned above in Section 2, of the Ce-activated sample. Since phosphorescence is characterized by a long decay time, its intensity quickly saturates at intense excitation, and its proportion decreases with increasing the excitation power. For this application, the presence of the phosphorescence is not critical as it is for applications where scintillators are used to detect ionizing radiation.

5. Conclusions

The potential of GYAGG:Tb (Ce) quaternary garnet scintillators for use in indirect betavoltaics has been investigated. Spectroscopic studies were carried out with various excitation sources, including a 150 keV electron beam, with the highest intensity corresponding to the typical activity of the 100% enriched isotopes (^{63}Ni, ^{147}Pm, and ^{14}C) used in this field. It has been established that under intense excitation, the saturation of the scintillation yield occurs due to quenching by the Auger mechanism. At the same time, notable saturation was not observed in the Ce-activated material, while in the terbium-activated material, it was measured at no more than 30%, which is confirmed by measuring both the scintillation kinetics and their integral yield. The Ce-activated scintillator was not codoped with magnesium and possessed phosphorescence. Its contribution to the integral yield was observed at low excitation power. Its contribution decreases with increasing excitation power, while its presence does not seem to be a critical factor for this scintillator application. Given the Tb-activated material's high initial scintillation yield [33], we conclude that it is prospective for use in indirect β-voltaic batteries.

Author Contributions: Conceptualization: I.K. (Ilya Komendo), M.K. and V.M.R.; Methodology: M.K., P.K. and A.V.; software: E.L., Y.T.; Investigation: A.F., I.K. (Irina Kamenskikh), D.K, D.T.; Data curation: V.P., V.S., V.M., A.V.; writing—original draft preparation: M.K. and A.V.; writing—review and editing: M.K., V.M.R. and A.V.; project administration: D.K. All authors have read and agreed to the published version of the manuscript.

Funding: This research received financial support from the Russian Federation represented by the Ministry of Education and Science of Russia, Agreement No. 075-15-2022-1157, dated 16 August 2022.

Institutional Review Board Statement: Not applicable.

Informed Consent Statement: Not applicable.

Data Availability Statement: Not applicable.

Acknowledgments: The authors at NRC "Kurchatov Institute" and Moscow State University acknowledge support from the Russian Ministry of Science and Education, Agreement No. 075-15-2021-1353. Analytical studies have been carried out using the scientific equipment of NRC Kurchatov Institute IREA. The research at Ural Federal University was partially supported by the Ministry of Science and Higher Education of the Russian Federation (Project FEUZ 2023-0013).

Conflicts of Interest: The authors have no conflict of interest to disclose.

References

1. Schmidt, G.; Sutliff, T.; Dudzinksi, L. Radioisotope power: A key technology for deep space exploration. *Radioisot.–Appl. Phys. Sci.* **2011**, 419–456.
2. Datas, A.; Martí, A. Thermophotovoltaic energy in space applications: Review and future potential. *Sol. Energy Mater. Sol. Cells* **2017**, *161*, 285–296. [CrossRef]
3. Olsen, L.; Cabauy, P.; Elkind, B. Betavoltaic power sources. *Phys. Today* **2012**, *65*, 35. [CrossRef]

4. Romer, M.; Miley, G.H.; Luo, N.; Gimlin, R.J. Ragone plot comparison of radioisotope cells and the direct sodium borohydride/hydrogen peroxide fuel cell with chemical batteries. *IEEE Trans. Energy Convers.* **2008**, *23*, 171–178. [CrossRef]
5. Prelas, M.A.; Weaver, C.L.; Watermann, M.L.; Lukosi, E.D.; Schott, R.J.; Wisniewski, D.A. A review of nuclear batteries. *Prog. Nucl. Energy* **2014**, *75*, 117–148. [CrossRef]
6. Spencer, M.; Alam, T. High power direct energy conversion by nuclear batteries. *Appl. Phys. Rev.* **2019**, *6*, 031305. [CrossRef]
7. Steinfelds, E.V.; Ghosh, T.K.; Prelas, M.; Tompson, R.V.; Loyalka, S.K. *The Research and Development of the Radioisotope Energy Conversion System*; University of Missouri: Columbia, MO, USA, 2001; ISSN 0003-018X.
8. Green, M.; Bremner, S. Energy conversion approaches and materials for high-efficiency photovoltaics. *Nat Mater.* **2016**, *16*, 23–34. [CrossRef] [PubMed]
9. Prelas, M.; Alam, T.; Tchouaso, M. Photovoltaics and nuclear energy conversion for space power: Background and issues. *Photovolt. Space* **2023**, 157–171.
10. Maximenko, S.; Moore, J.E.; Affouda, C.A.; Jenkins, P.P. Optimal semiconductors for 3H and 63Ni betavoltaics. *Sci. Rep.* **2019**, *9*, 10892. [CrossRef]
11. Korzhik, M.; Abashev, R.; Fedorov, A.; Dosovitskiy, G.; Gordienko, E.; Kamenskikh, I.; Kazlou, D.; Kuznecova, D.; Mechinsky, V.; Pustovarov, V.; et al. Towards effective indirect radioisotope energy converters with bright and radiation hard scintillators of (Gd, Y)$_3$Al$_2$Ga$_3$O$_{12}$ family. *Nucl. Eng. Technol.* **2022**, *54*, 2579–2585. [CrossRef]
12. Jarrell, J.; Cherepy, N.; Murphy, J.W.; Nikolic, R.J.; Swanberg, E.L., Jr. Indirect Conversion Nuclear Battery Using Transparent Scintillator Material. U.S. Patent 11415713, 16 August 2022.
13. Jarrell, J.; Cherepy, N.; Murphy, J.W.; Nikolic, R.J.; Swanberg, E.L., Jr. Indirect Conversion Nuclear Battery Using Transparent Scintillator Material. U.S. Patent 20220350039, 3 November 2022.
14. Gektin, A.; Korzhik, M. *Inorganic Scintillators for Detector Systems*; Springer: Berlin/Heidelberg, Germany, 2017.
15. Karipbayev, Z.T.; Kumarbekov, K.; Manika, I.; Dauletbekova, A.; Kozlovskiy, A.L.; Sugak, D.; Ubizskii, S.B.; Akilbekov, A.; Suchikova, Y.; Popov, A.I. Optical, structural, and mechanical properties of $Gd_3Ga_5O_{12}$ single crystals irradiated with 84Kr+ ions. *Phys. Status Solidi* **2022**, *259*, 2100415. [CrossRef]
16. Mironova-Ulmane, N.; Sildos, I.; Vasil'chenko, E.; Chikvaidze, G.; Skvortsova, V.; Kareiva, A.; Muñoz-Santiuste, J.; Pareja, R.; Elsts, E.; Popov, A. Optical absorption and Raman studies of neutron-irradiated $Gd_3Ga_5O_{12}$ single crystals. *Nucl. Instrum. Methods Phys. Res. Sect. B Beam Interact. Mater. At.* **2018**, *435*, 306–312. [CrossRef]
17. Pankratova, V.; Skuratov, V.A.; Buzanov, O.A. Radiation effects in Gd$_3$(Al, Ga)$_5$:O$_{12}$: Ce^{3+} single crystals induced by swift heavy ions. *Opt. Mater. X* **2022**, *16*, 100217. [CrossRef]
18. Jarrell, J.; Cherepy, N.J.; Seeley, Z.M.; Murphy, J.W.; Swanberg, E.L.; Voss, L.F.; Frye, C.D.; Stoyer, M.A.; Henderson, R.A.; O'Neal, S.P.; et al. Beta radiation hardness of GYGAG (Ce) transparent ceramic scintillators. *IEEE Trans. Nucl. Sci.* **2022**, *69*, 938–941. [CrossRef]
19. Alenkov, V.; Alenkov, V.; Buzanov, O.; Dosovitskiy, G.; Egorychev, V.; Fedorov, A.; Golutvin, A.; Guz, Y.; Jacobsson, R.; Korjik, M.; et al. Irradiation studies of a multi-doped $Gd_3Al_2Ga_3O_{12}$ scintillator. *Nucl. Instrum. Methods Phys. Res. Sect. A* **2019**, *916*, 226–229. [CrossRef]
20. Auffray, E.; Auffray, E.; Dosovitskiy, G.; Fedorov, A.; Guz, I.; Korjik, M.; Kratochwill, N.; Lucchini, M.; Nargelas, S.; Kozlov, D.; et al. Irradiation effects on $Gd_3Al_2Ga_3O_{12}$ scintillators prospective for application in harsh irradiation environments. *Radiat. Phys. Chem.* **2019**, *164*, 108365. [CrossRef]
21. Dormenev, V.; Brinkmann, K.T.; Borisevich, A.; Kazlou, D.; Korzhik, M.; Moritz, M.; Novotny, R.W.; Orsich, P.; Gerasymov, I.; Tkachenko, S.; et al. Radiation tolerant YAG: Ce scintillation crystals grown under reducing Ar+ CO atmosphere. *Nucl. Instrum. Methods Phys. Res. Sect. A* **2021**, *1015*, 165764. [CrossRef]
22. Retivov, V.; Dubov, V.; Komendo, I.; Karpyuk, P.; Kuznetsova, D.; Sokolov, P.; Talochka, Y.; Korzhik, M. Compositionally disordered crystalline compounds for next generation of radiation detectors. *Nanomaterials* **2022**, *12*, 4295. [CrossRef]
23. Korjik, M.; Bondarau, A.; Dosovitskiy, G.; Dubov, V.; Gordienko, K.; Karpuk, P.; Komendo, I.; Kuznetsova, D.; Mechinsky, V.; Pustovarov, V.; et al. Lanthanoid-doped quaternary garnets as phosphors for high brightness cathodoluminescence-based light sources. *Heliyon* **2022**, *8*, e10193. [CrossRef]
24. De Leeuw, D.; Hooft, G. Method for the analysis of saturation effects of cathodoluminescence in phosphors; applied to Zn_2SiO_4: Mn and $Y_3Al_5O_{12}$: Tb. *J. Lumin.* **1983**, *28*, 275–300. [CrossRef]
25. Retivov, V.; Dubov, V.; Kuznetsova, D.; Ismagulov, A.; Korzhik, M. Gd^{3+} content optimization for mastering high light yield and fast $Gd_xAl_2Ga_3O_{12}$: Ce^{3+} scintillation ceramics. *J. Rare Earths* **2022**. [CrossRef]
26. Korzhik, M.; Retivov, V.; Bondarau, A.; Dosovitskiy, G.; Dubov, V.; Kamenskikh, I.; Karpuk, P.; Kuznetsova, D.; Smyslova, V.; Mechinsky, V.; et al. Role of the dilution of the Gd sublattice in forming the scintillation properties of quaternary (Gd, Lu)$_3$Al$_2$Ga$_3$O$_{12}$: Ce ceramics. *Crystals* **2022**, *12*, 1196. [CrossRef]
27. Kamada, K.; Yanagida, T.; Pejchal, J.; Nikl, M.; Endo, T.; Tsutumi, K.; Fujimoto, Y.; Fukabori, A.; Yoshikawa, A. Scintillator-oriented combinatorial search in Ce-doped (Y,Gd)$_3$(Ga,Al)$_5$O$_{12}$ multicomponent garnet compounds. *J. Phys. D Appl. Phys.* **2011**, *44*, 505104. [CrossRef]
28. Chewpraditkul, W.; Pattanaboonmee, N.; Chewpraditkul, W.; Kamada, K.; Yoshikawa, A.; Nikl, M. Luminescence and scintillation response of $YGd_2Al_2Ga_3O_{12}$:Ce and $LuGd_2Al_2Ga_3O_{12}$:Ce scintillators. *Radiat. Meas.* **2016**, *90*, 153–156. [CrossRef]

29. Robbins, D.J.; Cockayne, B.; Lent, B.; Glasper, J.L. The mechanism of 5D3− 5D4 cross-relaxation in $Y_3Al_5O_{12}$: Tb^{3+}. *Solid State Commun.* **1976**, *20*, 673–676. [CrossRef]
30. Duan, C.-K.; Ko, C.-C.; Jia, G.; Chen, X.; Tanner, P.A. 5D3–5D4 cross-relaxation of Tb^{3+} in a cubic host lattice. *Chem. Phys. Lett.* **2011**, *506*, 179–182. [CrossRef]
31. Agostinelli, S.; Allison, J.; Amako, K.A.; Apostolakis, J.; Araujo, H.; Arce, P.; Asai, M.; Axen, D.; Banerjee, S.; Barrand, G.J.N.I.; et al. Geant4—A simulation toolkit. *Nucl. Instrum. Methods Phys. Res. Sect. Accel. Spectrometers Detect. Assoc. Equip.* **2003**, *506*, 250–303. [CrossRef]
32. Korzhik, M.; Alenkov, V.; Buzanov, O.; Dosovitskiy, G.; Fedorov, A.; Kozlov, D.; Mechinsky, V.; Nargelas, S.; Tamulaitis, G.; Vaitkevičius, A. Engineering of a new single-crystal multi-ionic fast and high-light-yield scintillation material $(Gd_{0.5}–Y_{0.5})_3Al_2Ga_3O_{12}$: Ce, Mg. *CrystEngComm.* **2020**, *22*, 2502–2506. [CrossRef]
33. Korzhik, M.; Retivov, V.; Dosovitskiy, G.; Dubov, V.; Kamenskikh, I.; Karpuk, P.; Komendo, I.; Kuznetsova, D.; Smyslova, V.; Mechinsky, V.; et al. First Observation of the Scintillation Cascade in Tb^{3+} Doped Quaternary Garnet Ceramics. *Phys. Status Solidi (RRL)–Rapid Res. Lett.* **2022**, 2200368.